# Synthesis and Characterization of Nano-Crystalline Fluorine-Doped Tin Oxide Thin Films by Sol-Gel Method

A.N. BANERJEE, S. KUNDOO, P. SAHA AND K.K. CHATTOPADHYAY*
*Department of Physics, Jadavpur University, Calcutta 700 032, India*
kkc@juphys.ernet.in

**Abstract.** Thin films of fluorine-doped tin-oxide (FTO) were prepared by sol-gel dip-coating technique. Stannous chloride ($SnCl_2 \cdot 2H_2O$) and hydrogen fluoride (HF) were mixed with isopropyl alcohol to serve as source solution. X-ray diffraction (XRD) spectrum showed all the peaks of the crystalline $SnO_2$. Analysis of XRD spectrum showed the particle size to be nearly 6 nm, which indicated the nanocrystalline structure of the films. Strain calculation by integral breadth (IB) method from XRD data showed a value of 0.010. UV-Visible spectrophotometric measurement showed high transparency of the films in the visible region and the band gap was calculated to be 3.34 eV. The room temperature resistivity of the films were of the order of 1 $\Omega$cm. Fluorine concentration in the films was determined from energy dispersive X-ray (EDX) study. Current-voltage (I-V) characteristics at high temperatures showed the Poole-Frenkel effect of thermionic emission. SEM study indicated the existence of fine grains in the film. FT-IR spectroscopy showed strong Sn—O and Sn—O—Sn bonding.

**Keywords:** tin oxide, fluorine, nanocrystalline, Poole-Frenkel effect

## 1. Introduction

Tin-oxide is an *n*-type wide band-gap transparent material which has numerous applications in electronic devices, such as window layer of solar cells, electroluminescent devices, flat panel displays [1–4], substrate material in electrolysis, passive counter electrode for electrochromic devices [5], gas sensors [6], frost preventing surfaces [7], etc. In order to improve its optical and electrical properties, tin oxide films were doped with Molybdenum, Cadmium, Antimony (ATO) [8, 9], Fluorine (FTO) [10, 11] etc. Several methods were used for deposition of the films, which include chemical vapour deposition (CVD) [12–14], sputtering [12, 15, 16], thermal evaporation [17], pyrosol [10] and sol-gel-dip-coating technique (SGDC) [8, 9, 11]. SGDC method has several advantages over the other methods such as, it is a low-cost and simple process, precise control over doping level is easier, possibility of using high purity starting materials and coating of large and complex shaped substrates is also easier.

It appears from the literature survey that, there exists very few published work on FTO by SGDC route. Most of them had used fluorine rich organic complexes [11] or $NH_4F$ [18] as a fluorine source. In this work, we have used $SnCl_2 \cdot 2H_2O$ and HF as starting material because of its easy availability, low cost and furthermore, for greater degree of incorporation of fluorine atom in the $SnO_2$ matrix leading to uniformity of the film in terms of thickness and resistivity.

In the present paper we have aimed to study the effect of an optimum percentage of fluorine doping into the $SnO_2$ matrix which would give higher conductivity and hence improved electrical characteristics. Also we have studied various electrical and optical properties of the FTO films, and the results may help for tailored film preparation and the understanding of electron transport phenomenon in the FTO films.

*To whom all correspondence should be addressed.

## 2.  Experimental

SnCl$_2 \cdot$2H$_2$O (99.5%), HF (40%) and isopropyl alcohol (99.8%) were taken as starting material. Several solutions were made by taking F:Sn atomic ratio, ranging from 25:1 to 64:1 in the starting solutions. The resulting solutions were stirred and refluxed for 1 hour at a temperature of ∼70°C and then aged for 2 hrs to form the sol. Ultrasonically cleaned glass slides and silicon substrates were first dipped into and then withdrawn vertically from the solution slowly at the rate of 8 cm/min for 10 to 15 times. Between two successive dipping the substrate along with the sol was dried at ∼80°C–100°C to have quick geletion. Thus the films were deposited layer by layer to achieve uniformity. After the dipping and withdrawing procedure the resulting films were annealed at ∼300°C–325°C in air for half an hour to form the required FTO films.

The deposited films were subjected to X-ray diffraction (XRD, by Cu K$\alpha$ line), scanning electron microscopy (JEOL-5200), Fourier-transform infrared spectroscopy (NICOLET MAGNA—750) analyses to examine the film morphology and structural properties. Film composition (Sn, O, F) was determined by energy dispersive X-ray analysis (EDX, Leica S-440, Oxford-ISIS), which could detect element from Boron (5) to Uranium (92). Optical transmittance was measured by a UV-VIS spectrophotometer (HITACHI-U3410). Temperature dependence of electrical conductivity of the films was studied by standard four probe method. For electrical measurement evaporated In electrodes were deposited and annealed at 150°C for 30 min to serve as ohmic contact.

## 3.  Results and Discussion

### 3.1.  Structural Properties

Figure 1 shows the X-ray diffraction pattern of a typical SnO$_2$:F film deposited on a 3.5 × 2.5 cm$^2$ glass substrate (without background correction). The peaks are identified to originate from (110), (101), (211), (220) and (301) reflections of tetragonal SnO$_2$ crystal structure [19]. Previous studies showed that SnO$_2$ films deposited from divalent tin salts such as SnCl$_2$ exhibited a strong (110) orientation [20]. However, as the thickness of the present film is small (∼0.5 $\mu$m) and the grain size is of the order of several nanometers, the peaks are broad and preferred orientation is not conclusively seen.
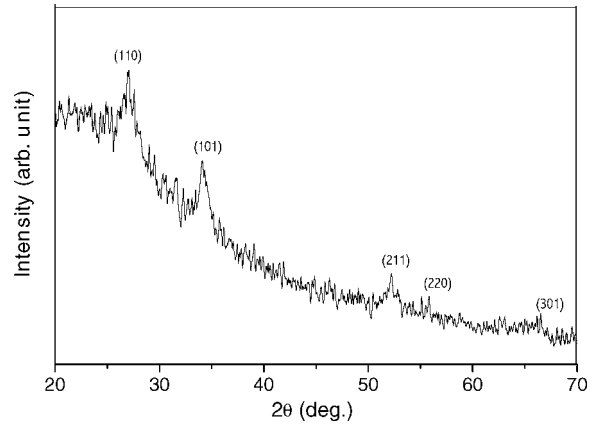


*Figure 1.*   XRD patterns of the SnO$_2$:F films on glass substrate.

The information on strain and the particle size is obtained from the full-widths-at-half-maximum (FWHM) of the diffraction peaks. The FWHM's ($\beta$'s) can be expressed as a linear combination of the contributions of the strain ($\varepsilon$) and particle size ($L$) through the following relation [21]:

$$\beta \cos\theta/\lambda = 1/L + \varepsilon \sin\theta/\lambda. \qquad (1)$$

Figure 2 represents the plot of $\beta \cos\theta/\lambda$ vs. $\sin\theta/\lambda$. Slope of the line gives the amount of strain which comes out to be $10 \times 10^{-3}$ and the intercept on y-axis gives the particle size as ∼6 nm.

Scanning electron micrograph of the film is shown in Fig. 3. It shows the presence of uniform and dense microstructure apparently devoid of any cracks and voids,
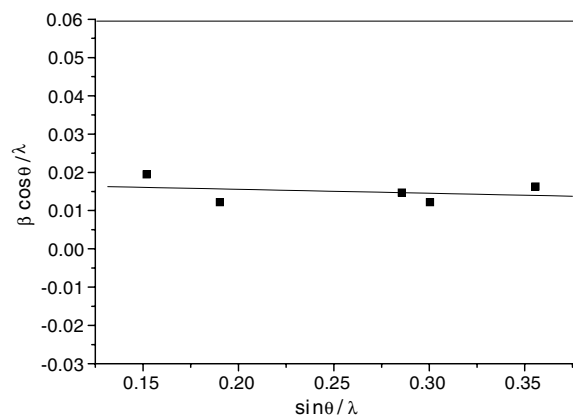


*Figure 2.*   Plot to determine strain and particle size of FTO films deposited on glass substrate. Data obtained from XRD pattern.
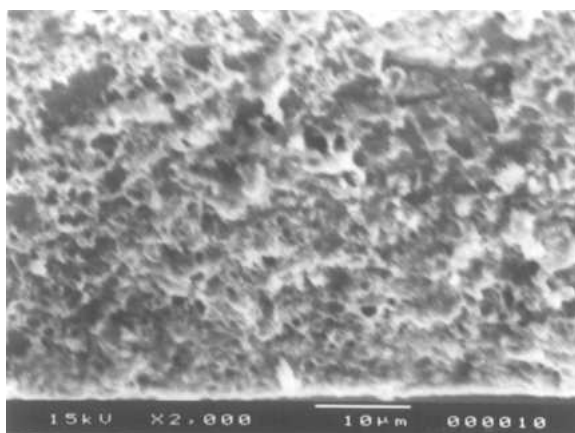
contamination. The sharp peak at 1081 cm$^{-1}$ is a Si—O peak which occurs due to the silicon substrate used. Si may be oxidized at the surface due to annealing of the film in air.

### 3.2. Compositional Analysis

The final fluorine content in the films is determined by energy dispersive X-ray analysis (EDX). It is seen that, the F/Sn atomic ratio inside the films is much lower than that was taken in the starting solution. For obtaining minimum resistivity in the deposited films, the presence of high concentration of F ions in the starting solution is required. It has been shown by other workers that the SnO$_2$:F film resistivity could be minimized if the F/Sn atomic ratio in the starting solution was as large as ~400% [11, 25, 26]. It can be noted that the corresponding F/Sn atomic ratio inside the film was much lower ranging from 1–3%. From Hall effect measurements, charge carrier concentration in the films with different fluorine contents is determined. It is found that, the amount of fluorine atoms acting as donors as calculated from Hall effect study, is lower than the EDX results. It means that there is an excess of fluorine, incorporated in interstitial positions and in grain boundary regions. The nominal composition in the starting solution, final composition in the films obtained from EDX results and the effective fluorine content determined from Hall effect study are listed in Table 1.

### 3.3. Optical and Electrical Properties

The optical transmission spectrum shown in Fig. 5 indicates that the film is highly transparent in the visible region. From the transmittance data, using Manifacier model [27] we have calculated absorption coefficients ($\alpha$) in the region of strong absorption. The fundamental absorption, which corresponds to electron excitation



*Figure 3.* SEM surface morphology indicating uniform and dense microstructure.
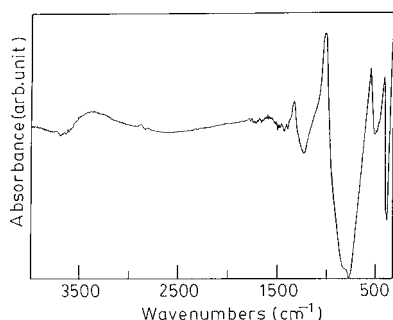


*Figure 4.* FT-IR spectra of FTO films on Si substrates indicating different Sn—O bonds.

although it is possible that some microscale porosity is present in the film. From the cross-sectional SEM study, the thickness of the film is determined to be ~0.5 $\mu$m.

Figure 4 represents the FT-IR spectrum of the SnO$_2$ film deposited on Si substrate. All bands have been assigned to the absorption peaks of Sn—O, Sn—O—Sn, Sn—OH or O—H bond vibrations. This suggests that our sol-gel derived FTO films do not contain any residual species such as chlorine ions or remaining propoxy groups. The absorption peaks between 400 cm$^{-1}$ to 700 cm$^{-1}$ are assigned to Sn—O and Sn—O—Sn vibrations of SnO$_2$. Small peaks between 1600 cm$^{-1}$– 1900 cm$^{-1}$ are attributed to Sn—OH vibrational mode [22–24]. Since the precursor solution contains water, Sn—OH vibrational mode appears in the spectrum. The broad peak near 3000 cm$^{-1}$–3500 cm$^{-1}$ is assigned to be due to O—H stretching vibration, which may be incorporated from the atmospheric moisture

*Table 1.* Nominal and final composition of the SnO$_2$:F films.

| Film no. | Nominal F:Sn atomic ratio | F/Sn atomic ratio in the film from EDX data (%) | Effective F/Sn atomic ratio in the film from Hall study (%) |
|---|---|---|---|
| S-18 | 25:1 | 1.62 | 0.025 |
| S-10 | 51:1 | 10.8 | 7.11 |
| S-15 | 64:1 | 12 | 3.77 |
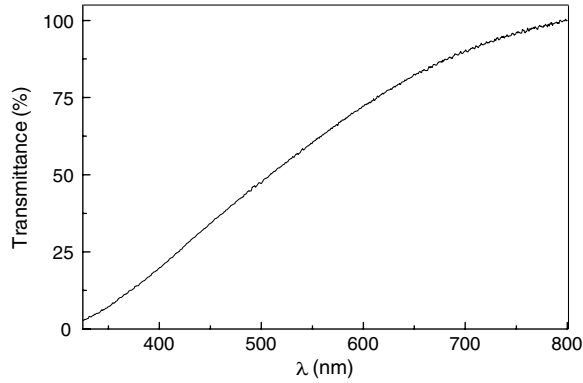
*Figure 5.* Optical transmission of FTO films deposited on glass substrates.



*Figure 7.* Temperature dependence of electrical conductivity of FTO thin films with F/Sn atomic ratio as (a) 10.8%, (b) 1.62%, and (c) 12%.

from the valance band to conduction band, can be used to determine the nature and value of the optical band gap. As the film is crystalline in nature, the relation between the absorption coefficients ($\alpha$) and the incident photon energy ($h\nu$) can be written as [28],

$$(\alpha h\nu)^2 = A(h\nu - E_g) \qquad (2)$$

where $A$ is a constant and $E_g$ is the band gap of the material. The $(\alpha h\nu)^2$ vs. $h\nu$ plot is shown in the Fig. 6. Extrapolating the linear portion of the graph to the $h\nu$ axis, we have obtained the direct band gap from the intercept, which is equal to 3.34 eV. Our band gap value is comparable with the value obtained by previous workers for their sol-gel derived $SnO_2$ films [22, 29]. The reported band gap values for $SnO_2$ thin

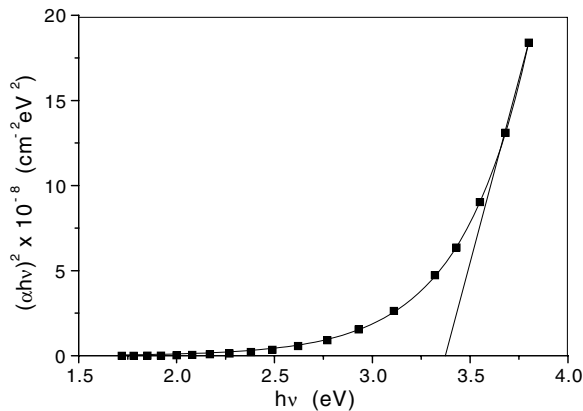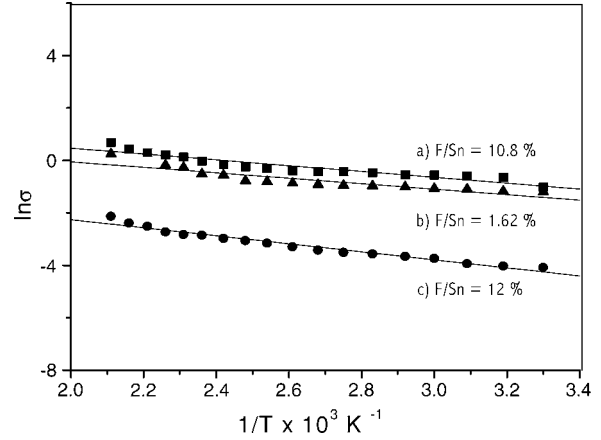films are between 3.3 and 4.0 eV and for single crystal 3.6 eV [30].

Figure 7 represents $\ln \sigma$ vs. $1/T$ plots of FTO films for different doping concentrations. The straight line nature of the Arrhenius plots indicates the thermally activated conduction as often found in doped semiconductors. From the slope of the line we get the value of activation energy ($E_a$) which corresponds to the minimum energy required to transfer electrons from donor level to the conduction band and the value of $E_a$ comes out to be 130, 85 and 90 meV for F/Sn atomic ratio as 12%, 10.8% and 1.62% respectively in the films. The minimum resistivity of our F doped $SnO_2$ films ($\sim$1 $\Omega$cm) is lower than that obtained by Catchet et al. [11] ($\sim$20 $\Omega$cm) but higher than Ray et al. [18] ($\sim$10$^{-2}$ $\Omega$cm). It is seen that the minimum resistivity has been achieved for an optimum F/Sn atomic ratio in the film (10.8%), above and below which resistivity increases. At F/Sn atomic ratio greater than 10.8%, it is seen from Hall effect data that the effective donor concentration decreases. This means excess fluorine atoms may be incorporated at the grain boundary or at interstitial positions which do not act favorably in conduction mechanism. Activation energies also decrease with the increase of effective fluorine content in the films.

Figure 8 gives the I-V characteristics of the FTO film with F/Sn atomic ratio = 10.8%, at different temperatures. The curves are non-linear in nature. Non-linearity is significant above 20 V. This is due to the presence of an electron depleted layer at the grain boundary and the formation of a potential barrier. This shape
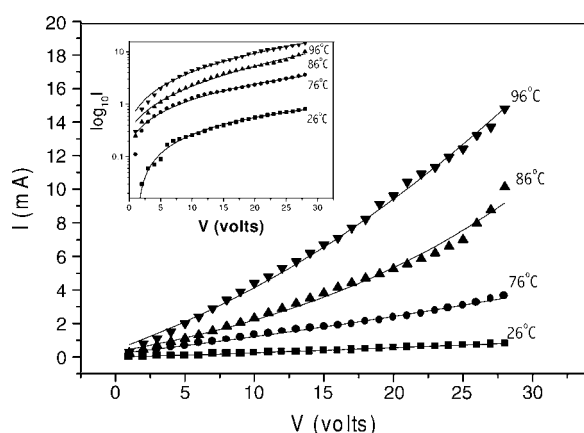


*Figure 6.* Test for direct bandgap transition for FTO films on glass substrate.

*Figure 8.*   Current-voltage characteristics of FTO films with F/Sn atomic ratio of 10.8% at several temperatures. Inset: Representation of the Poole-Frenkel model of thermionic emission.

of I-V curve is typical of thermionic emission over the barrier, explained by the Poole-Frenkel model of thermionic emission [31]. With the increase in temperature the curves show more and more deviation from ohmic behavior. The inset of Fig. 8 represents a test for Poole-Frenkel model of thermionic emission. For the films with smaller fluorine content the non-linear behavior in the I-V characteristics is also observed (not shown here), but the nonlinearity starts at higher voltages. For example, for the film with F/Sn atomic ratio = 1.62%, non-linear behavior of the I-V characteristics starts at ~100 V. This shift to higher starting voltages of the non-linear behavior could be explained with the increase in resistivity and activation energy of the films having lower F/Sn atomic ratio.

## 4.   Conclusions

Doping concentration in FTO thin films is a major parameter, which influences the electrical conductivity of the films. It is observed that an optimum F/Sn atomic ratio (10.8%) yields highest conductivity. Current-voltage relationship shows non-linear behavior, which can be described by Poole-Frenkel model of thermionic emission through grain boundary. Spectral dependence of the absorption coefficient indicates a direct bandgap of about 3.34 eV. The present work shows that FTO films of low sheet resistance can be prepared by using relatively inexpensible metal salts and fluorine sources rather than highly expensive alkoxides and fluorine rich organic complexes.

## References

1. C.M. Lampert, Sol. Ener. Mater. **6**, 1 (1981).
2. J.R. Bellingham, W.A. Philips, and C.J. Adkins, J. Mater. Sci. Lett. **11**, 263 (1992).
3. K. Omura, P. Veluchamy, M. Tsuji, T. Nishio, and D. Murojono, J. Electrochem. Soc. **146**, 2113 (1999).
4. S.J. Laverty, H. Feng, and P. Maguire, J. Electrochem. Soc. **144**, 2165 (1997).
5. P. Varshney, M. Deepa, N. Sharma, S.R. Gupta, B.B. Sharma, and S.A. Agnihotry, in *Ion Conducting Materials: Theory and Applications*, edited by A.R. Kulkarni and P. Gopalan (Narosa Publishing House 82, 2001).
6. A.V. Tadeev, G. Delabouglise, and M. Labeau, Mater. Sci. Engg. B **57**, 76 (1998).
7. Z. Hamberg, J.S.E.M. Svesson, T.S. Eriksson, C.G. Granqvist, P. Arrenius, and F. Narin, Appl. Opt. **26**, 2131 (1987).
8. C. Terrier, J.P. Chatelon, J.A. Roger, R. Berjoan, and C. Dubois, J. Sol-Gel Sci. Technol. **10**, 75 (1997).
9. D. Burgard, C. Goebbert, and R. Nass, J. Sol-Gel Sci. Technol. **13**, 789 (1998).
10. P. Veluchamy, M. Tsuji, T. Nishio, T. Aramoto, H. Higuchi, S. Kumazawa, S. Shibutani, J. Nakajima, T. Arita, H. Ohyma, A. Hanafusa, T. Hibino, and K. Omura, Sol. Eng. Mater. Sol. Cells **67**, 179 (2001).
11. H. Cachet, A. Gamard, G. Campet, B. Jousseaume, and T. Toupance, Thin Solid Films **388**, 41 (2001).
12. L.I. Popova, M.G. Mikhailov, V.K. Gueorguiev, and A. Shopov, Thin Solid Films **186**, 107 (1990).
13. J. Proscia and R.G. Gordon, Thin Solid Films **214**, 175 (1992).
14. S. Suh, Z. Zhang, W.K. Chu, and D.M. Hoffman, Thin Solid Films **345**, 240 (1999).
15. A. Czapla, E. Kusior, and M. Bucko, Thin Solid Films **182**, 15 (1989).
16. T. Suzuki, T. Yamazaki, and H. Oda, J. Mater. Sci. **24**, 1383 (1989).
17. Y.S. He, J.C. Campbell, R.C. Murphy, M.F. Arendt, and J.S. Swinnea, J. Mater. Res. **8**, 3131 (1993).
18. S.C. Ray, M.K. Karanjai, and D. Dasgupta, Surf. Coat. Technol. **102**, 73 (1998).
19. JCPDS Powder Diffraction File Card 5-0467.
20. A. Smith, J.M. Laurant, D.S. Smith, J.P. Bonnet, and R.R. Clemente, Thin Solid Films **266**, 20 (1995).
21. S.B. Quadri, E.F. Skelton, D. Hsu, A.D. Dinsmore, J. Yang, H.F. Gray, and B.R. Ratna, Phy. Rev. B **60**, 9191 (1999).
22. Z. Gu, P. Liang, X. Liu, W. Zhang, and Y. Le, J. Sol-Gel Sci. Technol. **18**, 159 (2000).
23. K. Nakamoto (Ed.), *Infrared Spectra of Inorganic and Coordinated Compounds* (John Wiley & Sons, Inc., 1963), p. 76, 86.
24. A. Finich, P.N. Gates, and K. Radcliffe (Eds.), *Chemical Application of Far Infrared Spectroscopy* (Academic Press, 1970), p. 200.

25. M. Fantini and I. Toriani, Thin Solid Films **138**, 255 (1986).
26. C. Agashe, M.G. Takwale, B.R. Marathe, and V.G. Bhide, Sol. Ener. Mat. Sol. Cells. **17**, 99 (1988).
27. J.C. Manifacier, M. De Murcia, J.P. Fillard, and E. Vicario, Thin Solid Films **41**, 127 (1977).
28. Pankove (Ed.), *Optical Processes in Semiconductors* (Prentice-Hall, Inc., 1971), p. 34.
29. J.P. Chatelon, C. Terrier, and J.A. Roger, J. Sol-Gel Sci. Technol. **10**, 55 (1997).
30. J.E. Dominquez, X.Q. Pan, L. Fu, P.A. Van Rompay, Z. Zhang, J.A. Nees, and P.P. Pronko, J. Appl. Phys. **91**, 1060 (2002).
31. K.L. Chopra, *Thin Film Phenomenon* (McGraw-Hill, New York, 1969), p. 502.